Available online at www.sciencedirect.com

ScienceDirect

Solar Energy 133 (2016) 207–220

SOLAR ENERGY

www.elsevier.com/locate/solener

Thermal performance of a PCM-filled double-glazing unit with different thermophysical parameters of PCM

Dong Li [a,*], Zaiwu Li [a], Yumeng Zheng [a], Changyu Liu [a], Ahmed Kadhim Hussein [b], Xiaoyan Liu [a]

[a] School of Architecture and Civil Engineering, Northeast Petroleum University, Daqing, People's Republic of China
[b] College of Engineering, Mechanical Engineering Department, University of Babylon, Babylon, Hilla, Iraq

Received 14 December 2015; received in revised form 15 February 2016; accepted 17 March 2016

Communicated by: Associate Editor Bibek Bandyopadhyay

Abstract

Application of phase change material (PCM) in the glazing structure can improve its thermal performance by enhancing its thermal energy storage capacity. In this study, the effect of thermophysical parameters of PCM on thermal performance of a PCM-filled double-glazing unit was investigated. The results show that the temperature time lag of the PCM-filled double-glazing unit increases and the temperature decrement factor decreases with the increase of density, thermal conductivity, specific heat capacity, latent heat, and melting temperature of PCM. Increasing density, latent heat, and melting temperature of PCM are effective to enhance the thermal performance of PCM-filled double-glazed units; however, enhancing thermal conductivity and specific heat capacity are ineffective when thermal conductivity is beyond 2.1 W/(m K) and specific heat capacity is < 4460 J/(kg K).

Keywords: Double-glazing unit; PCM; Thermophysical parameters

1. Introduction

Glazing unit is an indispensable part of a building, which provides passive solar energy gain and air ventilation (Martin et al., 2013; Erdem et al., 2014; Kimmo et al., 2015). However, in general, thermal performance of glazing units is poor among the building components, and hence they play a significant role in energy consumption of buildings. Effect of glazing units on energy loss from building envelope becomes much more drastic when the glazing area is large, for example, the heat loss through the glazing envelope is accounted for 30% of energy consumption of the building envelope (Erdem and Riffat, 2015; Hee et al., 2015). The thermal performance of a glazing unit is a property of glazing structure, which enables it to store heat, providing inertia against temperature fluctuations within a building.

It is widely accepted that good thermal performance is beneficial to buildings to increase thermal comfort and reduce energy consumption (Gowreesunker et al., 2013). There are several methods to improve thermal performance of glazing units, such as optimizing the air layer thickness of double glazing (Arıcı and Karabay, 2010), filling the cavity between panes with a participating gas (Ron et al., 2014), water (Chow et al., 2011) or aerogel (Takeshi et al., 2015), coating pane surface with low-emissivity materials (Erdem et al., 2015; Liao and Xu, 2015; Xamán et al., 2014), and using multiple pane windows (Aguilar et al., 2015; Müslüm et al., 2015, Müslüm and Mirac, 2015).

* Corresponding author. Tel.: +86 459 6507 763.
E-mail address: lidonglvyan@126.com (D. Li).

http://dx.doi.org/10.1016/j.solener.2016.03.039
0038-092X/

Nomenclature

A_{g1} solar absorptance of glass 1, –
A_{g2} solar absorptance of glass 2, –
A_{p1} solar absorptance of phase 1, –
A_{p2} solar absorptance of phase 2, –
$c_{P,g}$ specific heat of glass, J/(kg K)
$c_{P,p}$ specific heat of PCM, J/(kg K)
f_g temperature decrement factor, –
F_{sky} view factor between the glazing unit and sky dome, –
F_{ground} view factor between glazing unit and surrounding, –
H specific enthalpy of PCM, kJ/kg
h_{out} convective heat transfer coefficient of exterior surface of outer glass, W/(m^2 K)
h_{in} convective heat transfer coefficient of inner surface of internal glass, W/(m^2 K)
I_{sol} solar radiation, W/m^2
$I_{g\rightarrow p}$ radiative heat flux of coupled surface between outer glass and PCM, W/m^2
$I_{p,l\rightarrow p,s}$ radiative heat flux of liquid–solid interface in the PCM region, W/m^2
$I_{p\rightarrow g}$ radiative heat flux of coupled surface between internal glass and PCM, W/m^2
k_g thermal conductivity of glass, W/(m K)
k_p thermal conductivity of PCM, W/(m K)
$k_{p,l}$ thermal conductivity of liquid PCM near to liquid–solid interface, W/(m K)
$k_{p,s}$ thermal conductivity of solid PCM near to liquid–solid interface, W/(m K)
L_{g1} thickness of glass 1, m
L_{p1} thickness of phase 1, m
L_{p2} thickness of phase 2, m
L_{g2} thickness of glass 2, m
n_g refractive index of glass, –
n_{p1} refractive index of phase 1, –
n_{p2} refractive index of phase 2, –
$S(t)$ thickness of liquid PCM, m
Q_L latent heat of PCM, kJ/kg
q_{rad} radiative heat flux between exterior surface of outer glass with outdoor environment, W/m^2
$q_{rad,air}$ radiative heat flux between exterior surface of outer glass with air, W/m^2
$q_{rad,sky}$ radiative heat flux between exterior surface of outer glass with sky, W/m^2
$q_{rad,ground}$ radiative heat flux between exterior surface of outer glass with ground, W/m^2
T_{g1} solar transmittance of glass 1, –
T_{p1} solar transmittance of phase 1, –
T_{p2} solar transmittance of phase 2, –
T_{g2} solar transmittance of glass 2, –
$T_{g,max}$ maximum temperature on interior surface of double-glazing unit in temperature waves, K
$T_{g,min}$ minimum temperature on interior surface of double-glazing unit in temperature waves, K
$T_{a,max}$ maximum temperature of outdoors air in the temperature waves, K
$T_{a,min}$ minimum temperature of outdoors air in the temperature waves, K
T temperature, K
T_s temperature that the phase of PCM starts to change from solid to liquid, K
T_l temperature that PCM completely changed into liquid, K
T_g temperature of the coupled surface of outer glass, K
T_p temperature of coupled surface of PCM, K
T_{ref} reference temperature, K
$T_{p,l}$ temperature of liquid PCM near to liquid–solid interface, K
$T_{p,s}$ temperature of solid PCM near to liquid–solid interface, K
T_{out} temperature of the exterior surface of outer glass, K
$T_{a,out}$ temperature of ambient, K
T_{sky} sky temperature, K
T_{in} temperature of inner surface of internal glass, K
$T_{a,in}$ temperature of indoors air, K

Greek letters

α_g extinction coefficient of glass, m^{-1}
α_{p1} extinction coefficient of phase 1, m^{-1}
α_{p2} extinction coefficient of phase 2 of PCM, m^{-1}
β liquid fraction, –; a factor that splits the heat exchange with sky dome between sky and air radiation, –
ρ_g density of glass, kg/m^3
ρ_p density of PCM, kg/m^3
ρ_1 interface surface reflectance between air and glass, –
ρ_2 surface reflectance between phase 1 and glass, –
ρ_3 interface surface reflectance between phase 1 and phase 2 of PCM, –
ρ_4 interface surface reflectance between phase 2 of PCM and glass, –
τ time, s
$\tau_{g,max}$ time at the interior surface maximum temperature of the double-glazing unit, –
$\tau_{a,max}$ time at maximum temperature of outdoors environment, –
$\varnothing$ radiative source term, W/m^3

ε	surface emissivity of glass, –	*Subscript*	
σ	Stefan–Boltzmann constant, 5.670×10^{-8} W/(m^2 K^4)	a	air, –
		Con	convective
θ	angle between the glazing unit and the ground, –	g, p	glass and PCM, –
φ_g	temperature time lag of the double-glazing unit comparing with the outdoors air, min	in, out	inner surface and exterior surface, –
		Rad	radiative, –
		Sol	solar radiation intensity, –
		l, s	liquid and solid PCM, –

Another alternative practice to enhance thermal performance of glazing units is to increase their thermal storage capacity, which offers improved heat transfer control, resulting in reduced energy use and demand, enhanced occupant comfort, and increased operating life of the equipment. An effective approach to increase the thermal storage capacity of glazing units is to incorporate phase change material (PCM) in the glazing structure (Pielichowska and Pielichowski, 2014; Tiago et al., 2015a, b). The aim of the PCM-filled glazing unit concept is thus to absorb part of the solar energy for thermal energy storage, while letting visible light to enter the indoor environment for daylighting. Therefore, a variety of numerical and experimental work of thermal energy storage solutions for the integration of PCM into glazing units have been developed, which have attracted increasing attention as a potential technique for minimizing energy consumption in the buildings (Goia et al., 2012a,b, 2014a,b, 2015; Gowreesunker et al., 2013; Ismail and Henrıquez, 2002; Ismail et al., 2008; Li et al., 2014; Zhong et al., 2015).

Ismail and Henrıquez (2002) experimentally investigated the optical and thermal performances of glass windows filled with PCM (PCMWs) and found that their transmittance (~50%) and reflectance significantly decrease in the presence of infrared and ultraviolet radiations while maintaining good visibility compared with filling air, and that the increase in the thickness of the PCM layer has a marginal impact on the energy transmitted from the optical view point, however the thermal effect on the glass windows is very obvious. Ismail et al. (2008) also developed a one-dimensional radiation and heat conduction model of double PCMWs and found that its solar heat gain coefficient lies in the range of 0.65–0.80, when the external and internal ambient temperatures are 35 and 24 °C, respectively, and the incident solar radiation is 600 W/m^2.

Li et al. (2014) proposed two optical parameters to calculate the solar absorptance and transmittance of the PCMW and numerically investigated its thermal performance in the hot summer and cold winter areas of China. They found that in the representative sunny summer day, the peak temperature on the interior surface of the PCMW decreased by 10.2 °C, and the heat that entered the building through the PCMW decreased by 39.5% compared with the hollow window when its solar absorptance and transmittance are 0.19 and 0.76, respectively. Zhong et al. (2015) numerically investigated the effects of thermophysical parameters of PCM on the dynamic heat transfer of PCMW, including fusion latent heat, melting temperature, and temperature difference between the liquid and solid phases of PCM, and found that the thermal insulation and load-shifting effects of PCMW enhance by increasing the fusion latent heat of PCM and the optimal melting temperature of PCM applied in PCMW to 25–31 °C. Moreover, minimization of temperature difference between the liquid and solid phases could improve the thermal performance of PCMW. Goia et al. (2012a) introduced optical properties of PCM in solid and liquid states to a numerical model of heat transfer calculation in the glazing units filled with PCM, which describes the thermo-physical behavior of a PCM layer in combination with other transparent materials to perform numerical analyses on various PCM glazing units.

Goia et al. (2012b, 2014a,b, 2015) and Gowreesunker et al. (2013) significantly contributed to the fundamental aspect of thermal and optical properties of PCM glazing units. Goia et al. (2015, 2012b) measured the spectral and angular behavior of different glazing units filled with PCM that are characterized by different thicknesses of PCM using a commercial spectrophotometer and a dedicated optical test bed, and found that the relevant difference in the spectral feature of PCM can be observed when the PCM is in liquid and solid states. When the PCM is in the solid state, the reflectivity of the glazing units filled with PCM is far higher (up to thrice) than when it is in the liquid state. The absorption coefficient of glazing units filled with solid PCM is much higher than that of the liquid PCM. The thickness of the PCM layer has a major impact on the absorption coefficient and transmittance, but has an insignificant impact on the reflectivity. Goia et al. (2014a,b) developed a full-scale prototype of a PCM glazing system and analyzed its thermal performance. They found that the experimental results have highlighted a good ability of the PCM glazing units to store solar energy and smooth and delay peak values of the total heat flux. Gowreesunker et al. (2013) investigated the thermal and optical performance of a PCM-glazed unit using the T-history method and spectrophotometry principles, and also used the optical constants (i.e., extinction

coefficient and refractive index) to determine the optical properties of the PCM layer.

Recent studies have shown that optical performance of PCM in different phase state plays an important role in the thermal mass of PCM glazing units (Goia et al., 2012b, 2014a,b, 2015; Gowreesunker et al., 2013; Berthou et al., 2015), and the characterization of the thermal mass of the PCM layer affects considerably the thermal performance of the PCM glazing units. In fact, the thermophysical parameters of PCM play a key role in the phase state of PCM, which thus have an impact on the optical performance of PCM glazing units, and finally influence thermal mass of PCM glazing units. In this study, thermal performance parameters, such as density, specific heat capacity, latent heat, thermal conductivity, and melting temperature, of a PCM-filled double-glazing unit with different thermophysical parameters of PCM in Northeast China were numerically investigated under the different effect on optical performance of PCM in solid and liquid phase states.

2. Physical and mathematical models

2.1. Geometric description

Fig. 1 shows the details of the modeling double-glazing unit filled with PCM. It is evident from the figure that solar energy reaching the glazing unit surface is partly transmitted and partly reflected, and the remaining portion is absorbed by the two glasses and the PCM layer. The heat transfer process with the combination of thermal radiation and convection takes place on the boundary of the exterior and interior surfaces, respectively. The absorbed heat will be transmitted inward and/or outward by the processes of conduction, convection, and radiation exchange. For a transparent layer, the effective transmittance as well as the front and back reflectances are quantified as the consequence of multiple reflections between the front and back surfaces, plus the effects of absorption through the layer.

2.2. Governing equations and boundary conditions

Assumptions for the mathematical model are as follows:

(1) Heat transfer through the glazing unit is simplified to one-dimensional unsteady heat transfer process.
(2) Convection within the PCM layer is neglected.
(3) Radiative exchange between the two glass surfaces facing the cavity filled with PCM is neglected too. The PCM of liquid and solid states is highly non-transparent to the long-wave radiation.
(4) The glass and PCM are considered thermally homogeneous and isotropic media, and the thermal properties of the materials are independent of temperature.
(5) The scattering effect of PCM is omitted.

For the double-glazing unit filled with PCM, the heat transfer is calculated in three regions as shown in Fig. 2, which are the outer glass layer, internal glass layer, and the middle PCM layer.

A one-dimensional unsteady energy equation for glass regions is given as

$$\rho_g c_{P,g} \frac{\partial T}{\partial \tau} = k_g \frac{\partial^2 T}{\partial x^2} + \varnothing, \tag{1}$$

where τ is time (s); T is temperature (K); ρ_g, k_g, and $c_{P,g}$ are density (kg/m^3), thermal conductivity (W/m K), and specific heat (J/kg K) of glass, respectively; and $\varnothing$ is radiative source term (W/m^3).

The one-dimensional unsteady energy equation for PCM region is given as

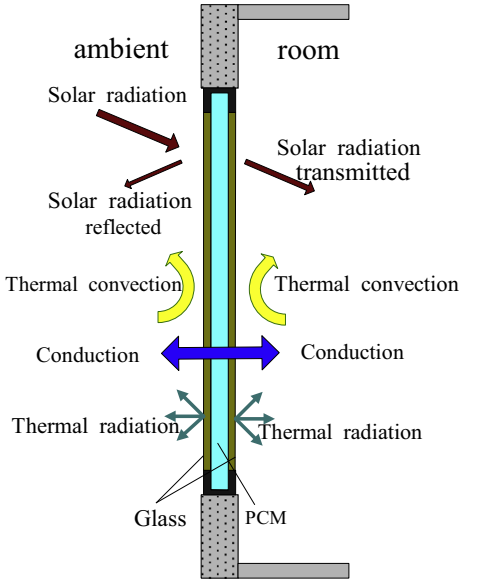

Fig. 1. Double-glazing unit filled with PCM.

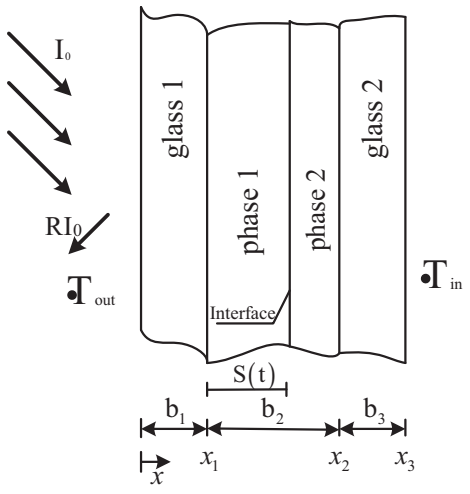

Fig. 2. Layout of double-glazing unit filled with PCM.

$$\rho_p \frac{\partial H}{\partial \tau} = k_p \frac{\partial^2 T}{\partial x^2} + \varnothing, \tag{2}$$

where H is the specific enthalpy of PCM (J/kg) and ρ_p and k_p are density (kg/m^3) and thermal conductivity (W/m K) of PCM, respectively.

The specific enthalpy of PCM in Eq. (2) is calculated by

$$H = \int_{T_{ref}}^{T} c_{P,p} dT + \beta Q_L \tag{3a}$$

$$\beta = 0, \quad T < T_s \tag{3b}$$

$$\beta = \frac{T - T_s}{T_l - T_s}, \quad T_s \leqslant T \leqslant T_l \tag{3c}$$

$$\beta = 1, \quad T > T_l, \tag{3d}$$

where T_{ref} is the reference temperature (K); $c_{P,p}$ is specific heat (J/kg K) of PCM; Q_L is the latent heat of PCM in the whole phase change process (kJ/kg); β is the local liquid fraction in the calculation region; and T_s and T_l are the temperatures at which the phase of PCM starts to change from solid to liquid (K) and completely changes to liquid (K), respectively.

The radiative source term for each layer is given as follows.

When the calculation node is in the glass 1 as shown in Fig. 2,

$$\varnothing = \frac{A_{g1} I_{sol}}{L_{g1}}. \tag{4a}$$

When the calculation node is in the phase 1 of PCM layer as shown in Fig. 2,

$$\varnothing = \frac{T_{g1} A_{p1} I_{sol}}{L_{p1}}. \tag{4b}$$

When the calculation node is in the phase 2 of PCM layer as shown in Fig. 2,

$$\varnothing = \frac{T_{g1} T_{p1} A_{p2} I_{sol}}{L_{p2}}. \tag{4c}$$

When the calculation node is in the glass 2 as shown in Fig. 2,

$$\varnothing = \frac{T_{g1} T_{p1} T_{p2} A_{g2} I_{sol}}{L_{g2}}, \tag{4d}$$

where I_{sol} is solar radiation (W/m^2); T_{g1}, T_{p1}, T_{p2}, and T_{g2} are solar transmittances of glass 1 layer, phase 1 layer, phase 2 layer, and glass 2 layer, respectively; A_{g1}, A_{p1}, A_{p2}, and A_{g2} are solar absorptances of glass 1 layer, phase 1 layer, phase 2 layer, and glass 2 layer, respectively; and L_{g1}, L_{p1}, L_{p2}, and L_{g2} are the thicknesses (m) of glass 1 layer, phase 1 layer, phase 2 layer, and glass 2 layer, respectively.

The transmittance and absorptance of the glass layer are calculated as (Li et al., 2015)

$$T_{g1} = \frac{(1-\rho_1)(1-\rho_2)\exp(-\alpha_g L_{g1})}{1-\rho_1\rho_2\exp(-2\alpha_g L_{g1})} \tag{5a}$$

$$A_{g1} = 1 - \rho_1 - \frac{(1-\rho_1)\rho_2\exp(-2\alpha_g L_{g1})}{1-\rho_1\rho_2\exp(-2\alpha_g L_{g1})} - T_{g1} \tag{5b}$$

$$T_{g2} = \frac{(1-\rho_1)(1-\rho_4)\exp(-\alpha_g L_{g2})}{1-\rho_1\rho_4\exp(-2\alpha_g L_{g2})} \tag{5c}$$

$$A_{g2} = 1 - \rho_4 - \frac{(1-\rho_4)\rho_1\exp(-2\alpha_g L_{g2})}{1-\rho_1\rho_4\exp(-2\alpha_g L_{g2})} - T_{g2}, \tag{5d}$$

where ρ_1, ρ_2, and ρ_4 are the interface reflectance for the surfaces between air and glass, phase 1 of PCM and glass, and phase 2 of PCM and glass, respectively, and α_g is the extinction coefficient of glass material (m^{-1}).

The transmittance and absorptance of the PCM layer are calculated as (Li et al., 2015)

$$T_{p1} = \frac{(1-\rho_2)(1-\rho_3)\exp(-\alpha_{p1} L_{p1})}{1-\rho_2\rho_3\exp(-2\alpha_{p1} L_{p1})} \tag{6a}$$

$$A_{p1} = 1 - \rho_2 - \frac{(1-\rho_2)\rho_3\exp(-2\alpha_{p1} L_{p1})}{1-\rho_2\rho_3\exp(-2\alpha_{p1} L_{p1})} - T_{p1} \tag{6b}$$

$$T_{p2} = \frac{(1-\rho_3)(1-\rho_4)\exp(-\alpha_{p2} L_{p2})}{1-\rho_3\rho_4\exp(-2\alpha_{p2} L_{p2})} \tag{6c}$$

$$A_{p2} = 1 - \rho_3 - \frac{(1-\rho_3)\rho_4\exp(-2\alpha_{p2} L_{p2})}{1-\rho_3\rho_4\exp(-2\alpha_{p2} L_{p2})} - T_{p2}, \tag{6d}$$

where ρ_3 is the interface reflectance for the surface between phases 1 and 2 of PCM and α_{p1} and α_{p2} are the extinction coefficients of phases 1 and 2 (m^{-1}), respectively.

The interface reflectances are calculated based on Fresnel's relations (Wang et al., 2013, 2014, 2015; Dai et al., 2014) as

$$\rho_1 = \frac{(n_g - 1)^2}{(n_g + 1)^2} \tag{7a}$$

$$\rho_2 = \frac{(n_g - n_{p1})^2}{(n_g + n_{p1})^2} \tag{7b}$$

$$\rho_3 = \frac{(n_{p1} - n_{p2})^2}{(n_{p1} + n_{p2})^2} \tag{7c}$$

$$\rho_4 = \frac{(n_g - n_{p2})^2}{(n_g + n_{p2})^2}, \tag{7d}$$

where n_g, n_{p1}, and n_{p2} are the refractive indices of glass material, phase 1 and phase 2 of PCM, respectively.

The mathematical boundary conditions for the calculation domain are given as follows.

In the exterior surface, the outer glass is exposed to solar radiation and the boundary condition at $x = 0$ is given as

$$-k_g \frac{\partial T}{\partial x} = q_{rad} + h_{out}(T_{out} - T_{a,out}), \tag{8}$$

where q_{rad} is radiative heat exchange between exterior surfaces of outer glass with the outdoor environment (W/m^2) and h_{out}, T_{out}, and $T_{a,out}$ are the convective heat transfer coefficient of the exterior surface of outer glass (W/m^2 K), temperature of the exterior surface of outer

glass (K), and ambient temperature (K), respectively. The radiative heat exchange with the outdoor environment q_{rad} is given by

$$q_{rad} = q_{rad,air} + q_{rad,sky} + q_{rad,ground}, \quad (9)$$

where $q_{rad,air}$, $q_{rad,sky}$, and $q_{rad,ground}$ are radiative heat fluxes for exchange with air, sky, and ground (W/m^2), respectively.

The radiation heat fluxes $q_{rad,air}$, $q_{rad,sky}$, and $q_{rad,ground}$ are respectively given by (Goia et al., 2012a)

$$q_{rad,sky} = \varepsilon\sigma F_{sky}\beta(T_{out}^4 - T_{sky}^4) \quad (10a)$$

$$q_{rad,air} = \varepsilon\sigma F_{sky}(1-\beta)(T_{out}^4 - T_{a,out}^4) \quad (10b)$$

$$q_{rad,ground} = \varepsilon\sigma F_{ground}(T_{out}^4 - T_{a,out}^4), \quad (10c)$$

where ε is the surface emissivity of glass, σ is the Stefan–Boltzmann constant, F_{sky} is the view factor between the glazing unit and the sky dome, F_{ground} is the view factor between the glazing unit and the surrounding surfaces, and all the surfaces are assumed to be at the same temperature, β is a factor that splits the heat exchange with the sky dome between sky and air radiation, T_{sky} is the sky temperature (K), and F_{sky}, F_{ground}, β, and T_{sky} are established by Goia et al. (2012a) as follows:

$$F_{sky} = \frac{1+\cos\theta}{2} \quad (11a)$$

$$F_{ground} = \frac{1-\cos\theta}{2} \quad (11b)$$

$$\beta = \sqrt{\frac{1+\cos\theta}{2}} \quad (11c)$$

$$T_{sky} = 0.0552 T_{a,out}^{1.5}, \quad (11d)$$

where θ is the angle between the glazing unit and the ground, for example, $\theta = 90°$ for a vertical glazing unit.

In the inner surface of internal glass near to indoor environment, the boundary condition at $x = x_3$ is given as (Ismail et al., 2008)

$$-k_g\frac{\partial T}{\partial x} = h_{in}(T_{in} - T_{a,in}) - \varepsilon\sigma(T_{in}^4 - T_{a,in}^4), \quad (12)$$

where h_{in}, T_{in}, and $T_{a,in}$ are the convective heat transfer coefficient of the inner surface of internal glass (W/m^2 K), temperature of the inner surface of internal glass (K), and indoor air temperature (K), respectively.

In the coupled surface between outer glass and PCM, when PCM is solid or liquid, the boundary condition at $x = x_1$ is given as (Ismail et al., 2008)

$$-k_g\frac{\partial T_g}{\partial x} + I_{g\to p} = -k_p\frac{\partial T_p}{\partial x}, \quad (13a)$$

where $I_{g\to p}$ is radiative heat flux of coupled surface between outer glass and PCM (W/m^2) and T_g and T_p are temperatures (K) of the coupled surface of outer glass and PCM, respectively.

In the coupled surface between outer glass and PCM, when the first liquid layer of the PCM near the internal face of the external glass sheet is formed, the boundary condition at $x = x_1$ is given as (Ismail et al., 2008)

$$-k_g\frac{\partial T_g}{\partial x} + I_{g\to p} = -k_p\frac{\partial T_p}{\partial x} + \rho_p H\frac{dS(t)}{dt}, \quad (13b)$$

where $S(t)$ is the thickness (m) of liquid PCM.

In the liquid–solid interface in the PCM region where the phase change occurs, the boundary condition at $x = x_1 + S(t)$ is given as (Ismail et al., 2008)

$$-k_{p,l}\frac{\partial T_{p,l}}{\partial x} + I_{p,l\to p,s} = -k_{p,s}\frac{\partial T_{p,s}}{\partial x} + \rho_p H\frac{dS(t)}{dt}, \quad (14)$$

where $I_{p,l\to p,s}$ is the radiative heat flux of liquid–solid interface in the PCM region (W/m^2); $T_{p,l}$ and $T_{p,s}$ are the temperatures (K) of liquid PCM near to liquid–solid interface and solid PCM near to liquid–solid interface, respectively; $k_{p,l}$ and $k_{p,s}$ are the thermal conductivities of liquid PCM near to liquid–solid interface and solid PCM near to liquid–solid interface (W/m K), respectively.

In the coupled surface between internal glass and PCM, when PCM is solid or liquid, the boundary condition at $x = x_2$ is given as (Ismail et al., 2008)

$$-k_p\frac{\partial T_p}{\partial x} + I_{p\to g} = -k_g\frac{\partial T_g}{\partial x}, \quad (15a)$$

where $I_{p\to g}$ is the radiative heat flux (W/m^2) of coupled surface between internal glass and PCM, respectively.

In the coupled surface between internal glass and PCM, when the first liquid layer of the PCM near to the internal glass sheet is formed, the boundary condition at $x = x_2$ is given as (Ismail et al., 2008)

$$-k_p\frac{\partial T_p}{\partial x} + I_{p\to g} + \rho_p H\frac{dS(t)}{dt} = -k_g\frac{\partial T_g}{\partial x}. \quad (15b)$$

Temperature time lag and temperature decrement factor are important parameters to analyze the thermal performance of the double-glazing unit. Temperature time lag is the phase difference of the temperature waves on the interior surfaces of the double-glazing unit, which is calculated by Eq. (16a). Temperature decrement factor is the ratio of the temperature waves on the interior surfaces of the amplitude of the double-glazing unit, which can be calculated by Eq. (16b). If the temperature time lag is high and temperature decrement factor is low, it means that the impact of the outdoor environment on the indoor thermal environment is small and the thermal performance of double-glazing unit is satisfactory (Li et al., 2014; Zhong et al., 2015):

$$\varphi_g = \tau_{g,max} - \tau_{a,max} \quad (16a)$$

$$f_g = \frac{T_{g,max} - T_{g,min}}{T_{a,max} - T_{a,min}}, \quad (16b)$$

where φ_g is the temperature time lag of the double-glazing unit compared with the outdoor air, $\tau_{g,max}$ is the time of the interior surface maximum temperature of the double-glazing unit, $\tau_{a,max}$ is the time of the maximum temperature in the outdoor temperature wave, f_g is the temperature decrement factor of the double-glazing unit compared with

the outdoors air, $T_{g,max}$ and $T_{g,min}$ are the maximum and minimum temperature on the interior surface of the double-glazing unit in the temperature waves, respectively, and $T_{a,max}$ and $T_{a,min}$ are the maximum and minimum temperature on the outdoor temperature wave, respectively.

2.3. Method of solution and validation of numerical procedure

The equations together with the boundary conditions are solved by using an explicit finite difference scheme as the procedure of reference (Goia et al., 2012a,b). PCM region is divided into 12 equally spaced increments. Each glass sheet is also divided into six equally spaced increments.

The numerical procedure is validated with the experimental parameters in the literature (Zhong et al., 2015). The outdoor air temperature, solar radiation intensity, and temperature on the interior surfaces of the PCM-filled double-glazing unit can be found as shown in Figs. 6–8 in Ref. Zhong et al. (2015). The thermophysical properties of materials can be found from Table 2 in Ref. Zhong et al. (2015). The extinction coefficient and refractive index of glass are 19 m^{-1} and 1.5 (Gowreesunker et al., 2013), respectively. The emissivity of the glass is 0.88 (Ismail et al., 2008). The refractive index of PCM is 1.3, and the extinction coefficients of solid and liquid PCMs are 50 and 40 m^{-1}, respectively (Gowreesunker et al., 2013). The initial temperature of the domain is 23 °C. The simulation was kept running until the solution becomes periodic, which needs 2 days to attain the periodic condition. The comparison of heat flux (without transmitted solar energy) and temperature on the interior surfaces of the PCM-filled double-glazing units between numerical results obtained in this study and the literature (Zhong et al., 2015) is shown in Fig. 3.

As shown in Fig. 3, the numerical and the literature results have different characteristics in different time. Before 7:00, the difference between numerical and the literature results is huge, and the reason is that the effect of initial temperature in the double-glazing units filled with PCM in the experiment is not omitted when heat conduction plays an important role in the heat transfer process; however, this effect is omitted in the calculation, because the calculation method could reach the rational periodic condition. In the time region 7:00–11:00, the numerical results agree well with those of the literature, and the reason is that the effect of initial temperature in the double-glazing units filled with PCM in the experiment can be eliminated after running 7 h, and both phase change of PCM and radiation transfer play an important role in this heat transfer process. However, in the time region 11:00–14:00, the difference between numerical and literature results is also high, because radiation transfer plays an important role in this heat transfer process when the phase of PCM is liquid in this time region. The exact optical parameters of PCM, which lead to a large numerical error, cannot be obtained. In the time region 14:00–22:00, the numerical results are in good agreement with those of the literature, because both phase change of PCM and radiation transfer play an important role in this heat transfer process.

3. Results and discussion

In this modeling work, thicknesses of the glass and PCM are 6 and 12 mm, respectively, and $\theta = 0$. The measured average hourly variations of the ambient air temperature and total radiation on June 22 in Daqing are shown in Fig. 4. The values of h_{out} and h_{in} are 7.75 and 7.43 W/m^2 K (Li et al., 2014), respectively. The indoor air temperature is 26 °C. The thermophysical properties of the materials are listed in Table 1. The extinction coefficient and refractive index of glass are 19 m^{-1} and 1.5 (Gowreesunker et al., 2013), respectively. The emissivity of the glass is 0.88 (Li et al., 2014). The refractive index of liquid and solid PCMs is 1.3, and the extinction coefficients of the solid and liquid PCMs are 30 and

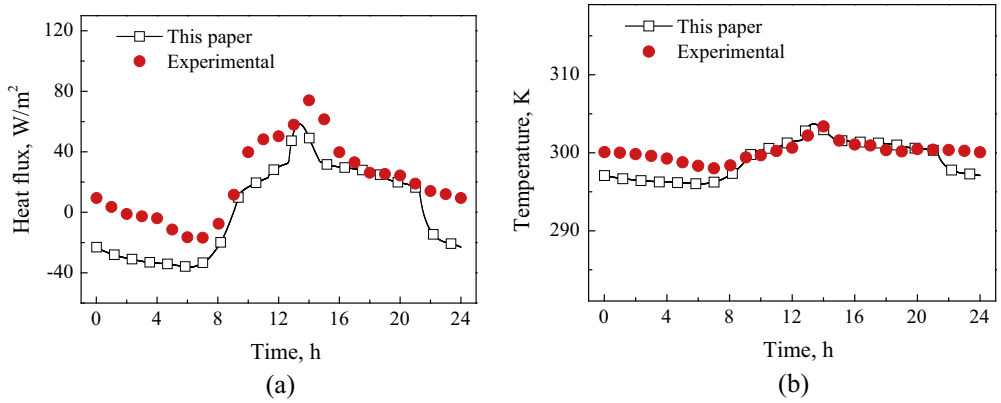

Fig. 3. Comparison of heat flux and temperature on the interior surfaces of the PCM-filled double-glazing units in this study and the literature (Zhong et al., 2015) (a: heat flux; b: temperature).

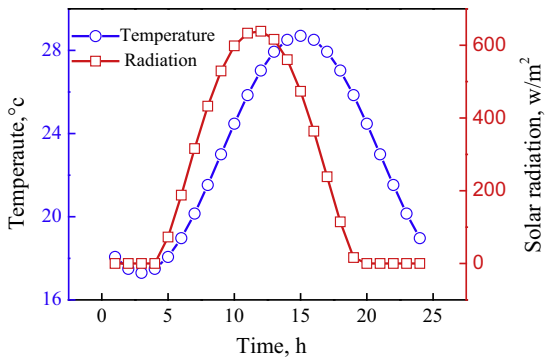

Fig. 4. Mean hourly variation of ambient temperature and solar energy.

5 m^{-1}, respectively. The initial temperature of the domain is 20 °C.

3.1. Effect of density

For investigating the effect of density of PCM on energy performance of glazing units containing PCM, the conditions of five types of density of PCM, $0.5\rho_p = 425$, $\rho_p = 850$, $1.5\rho_p = 1275$, $2\rho_p = 1700$, and $3\rho_p = 2550$ kg/m^3, are investigated, while keeping the remaining parameters unchanged as in Table 1.

Fig. 5 illustrates simulation results of the interior surfaces on double-glazed units with different density of PCM. As shown in Fig. 5(a), when the density of PCM is 425, 850, 1275, 1700, or 2550 kg/m^3, the temperature time lag and temperature decrement factor become 8 min and 1.00, 17 min and 1.00, 43 min and 0.98, 74 min and 0.94, and 75 min and 0.80, respectively. These results show that with the density of PCM increasing, the temperature time lag increases and the temperature decrement factor decreases; however, the effect of density of PCM on the temperature decrement factor is weak. From Fig. 5(b), it can be seen that with the density of PCM increasing, the transmitted energy of the interior surface on double-glazed units increases before 3:00 and after 20:00, but it decreases in the time range 3:00–20:00. The reason is that the solar energy plays a key role in the attribution of total transmitted energy in the double-glazed units as shown in

Table 1
Thermophysical properties of materials.

Material	Melting temperature (°C)	Density (kg/m^3)	Thermal conductivity (W/m K)	Specific heat capacity (J/kg K)	Latent heat (kJ/kg)
Glass	–	2500	0.96	840	–
PCM	27–29	850	0.21	2230	205

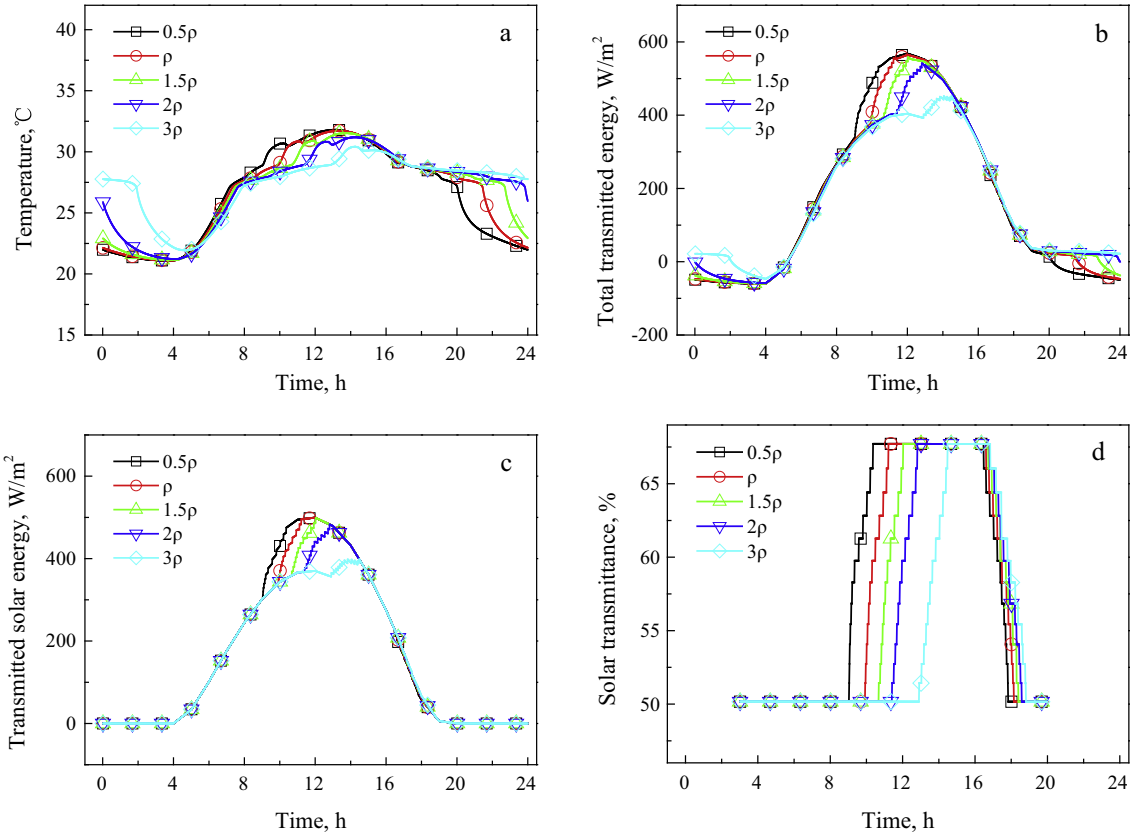

Fig. 5. Simulation results of the interior surface on double-glazed units with different density of PCM (a: temperature; b: total energy; c: solar energy; d: solar transmittance).

Fig. 5(c). With the density of PCM increasing, the stored solar energy of PCM increases, which results in the higher temperature before 3:00 and after 20:00 and lower temperature in the time range 3:00–20:00 as indicated in Fig. 5(a).

It is found from Fig. 5(d) that with the density of PCM increasing, the time when the PCM starts to melt is delayed, and the time range of liquid PCM decreases, which shows that the solar energy entering into room decreases with density of PCM increasing. For example, the initial melting time and the time range of liquid PCM with the density of PCM 425 and 2550 kg/m^3 are 9:03 and 366 min and 12:55 and 141 min, respectively. The above analysis indicates that choosing the rational density of PCM is an effective method to improve the thermal performance of double-glazed units filled with PCM; however, the time range of liquid PCM is much narrow when the density of PCM is beyond 1275 kg/m^3, which shows that the solar transmittance of double-glazed units filled with PCM is poor.

3.2. Effect of thermal conductivity

For investigating the effect of thermal conductivity of PCM on energy performance of glazing units containing PCM, the conditions of five types of thermal conductivity of PCM, $0.1k_p = 0.021$, $k_p = 0.21$, $10k_p = 2.1$, $100k_p = 21$, and $200k_p = 42$ W/m K are investigated, while keeping the remaining parameters unchanged as in Table 1.

Fig. 6 shows simulation results of the interior surfaces on double-glazed units with different thermal conductivity of PCM. As shown in Fig. 6(a), when the thermal conductivity of PCM is 0.021 W/m K, the temperature time lag and temperature decrement factor are −75 min and 0.90, respectively; when the thermal conductivity of PCM is 0.21 W/m K, 17 min and 1.00, respectively; when the thermal conductivity of PCM is 2.1 W/m K, 21 min and 1.11, respectively; when the thermal conductivity of PCM is 21 W/m K, 22 min and 1.13, respectively; when the thermal conductivity of PCM is 42 W/m K, the temperature time lag and temperature decrement factor are nearly the same as that for the thermal conductivity 21 W/m K, respectively. These results show that when the thermal conductivity of PCM is <2.1 W/m K, with the thermal conductivity of PCM increasing, the temperature time lag increases, and the temperature decrement factor decreases; however, when the thermal conductivity of PCM is beyond 2.1 W/m K, the effect of thermal conductivity of PCM on the temperature decrement factor is clearly very weak. From Fig. 6(b) and (c), it can be observed that the effect of thermal conductivity of PCM on the total transmitted and solar energy of the interior surface on double-glazed units is also weak when the thermal conductivity of PCM is

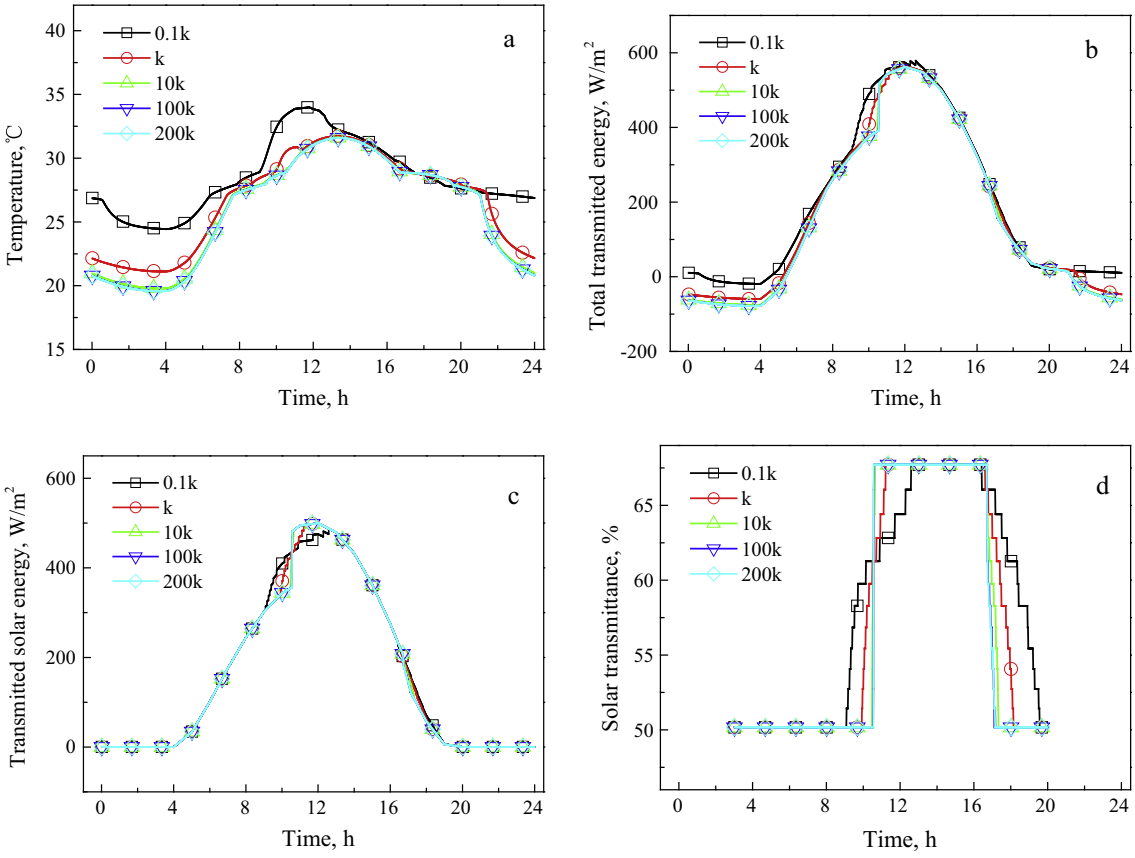

Fig. 6. Simulation results of the interior surface on double-glazed units with different thermal conductivities of PCM (a: temperature; b: total energy; c: solar energy; d: solar transmittance).

beyond 0.21 W/m K. The reason is that solar radiation plays an important role in heat transfer of the double-glazed units filled with PCM.

It can be seen from Fig. 6(d) that with the thermal conductivity of PCM increasing, the initial melting time is delayed, and the time range of liquid PCM increases; however, the thermal conductivity of PCM on the initial melting time and the time range of liquid PCM is very weak when the thermal conductivity of PCM is beyond 2.1 W/m K. For example, the initial melting time and the time range of liquid PCM with the thermal conductivities of PCM 0.021 and 2.1 W/m K are 9:06 and 229 min and 10:29 and 362 min, respectively. The above analysis indicates that increasing the thermal conductivity of PCM is not an effective method to improve the thermal performance of double-glazed units filled with PCM when the thermal conductivity of PCM is beyond 2.1 W/m K.

3.3. Effect of specific heat capacity

For investigating the effect of specific heat capacity of PCM on energy performance of glazing units containing PCM, the conditions of five types of specific heat capacity of PCM, $0.1c_{p,p} = 223$, $c_{p,p} = 2230$, $2c_{p,p} = 4460$, $5c_{p,p} = 11{,}150$, and $10c_{p,p} = 22{,}300$ J/kg K, are investigated, while keeping the remaining parameters unchanged as in Table 1.

Fig. 7 illustrates simulation results of the interior surfaces on double-glazed units with different specific heat capacity of PCM. As shown in Fig. 7(a), when the specific heat capacity of PCM is 223, 2230, 4460, 11,150, or 22,300 J/kg K, the temperature time lag and temperature decrement factor are 5 min and 1.01, 17 min and 1.00, 35 min and 0.98, 70 min and 0.90, and 101 min and 0.76, respectively. These results show that with the specific heat capacity of PCM increasing, the temperature time lag increases, and the temperature decrement factor decreases; however, the effect of specific heat capacity of PCM on the temperature decrement factor is weak when the specific heat capacity of PCM is <4460 J/kg K. From Fig. 7 (b) and (c), it can be seen that the effect of specific heat capacity of PCM on the total transmitted and solar energy of the interior surface on double-glazed units is also weak when the specific heat capacity of PCM is <4460 J/kg K.

It is found from Fig. 7(d) that with the specific heat capacity of PCM increasing, the initial melting time is delayed, and the time range of liquid PCM changes slightly; however, the specific heat capacity of PCM on the initial melting time and the time range of liquid PCM is very weak when the specific heat capacity of PCM is <4460 J/kg K. For example, the initial melting time and

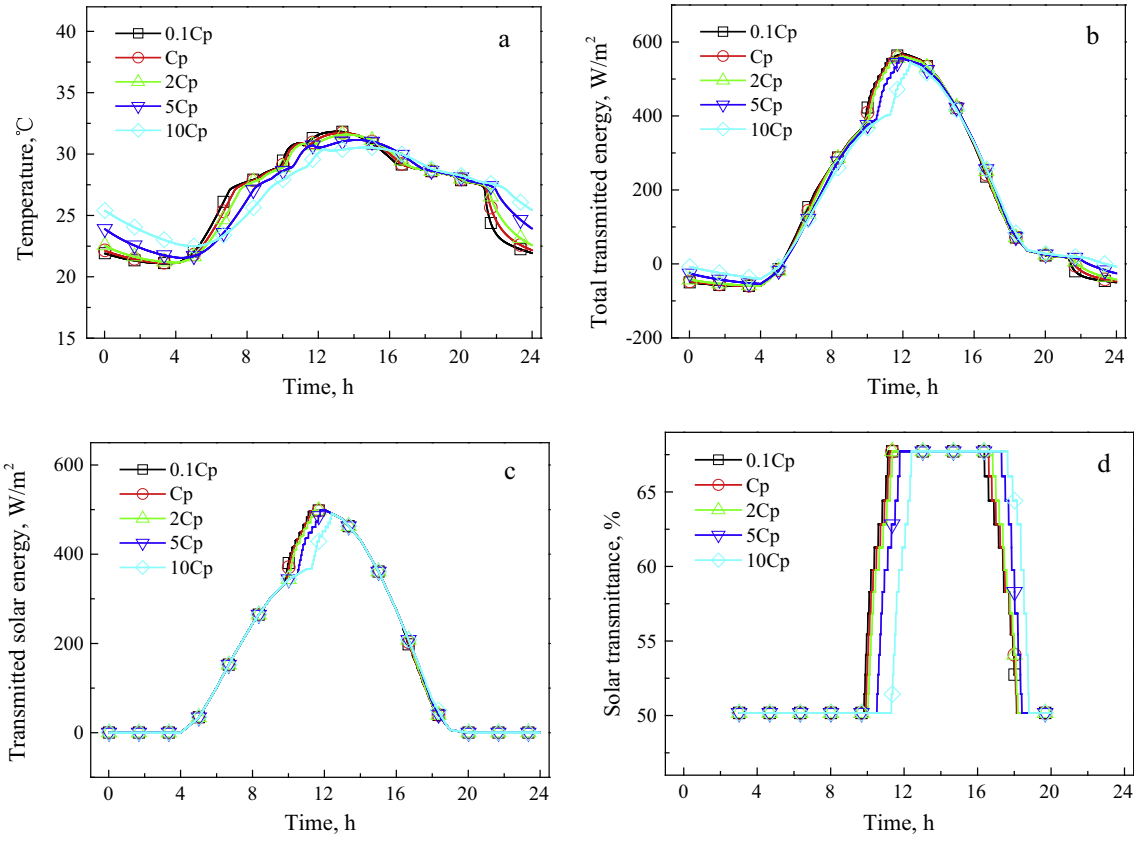

Fig. 7. Simulation results of the interior surface on double-glazed units with different specific heat capacities of PCM (a: temperature; b: total energy; c: solar energy; d: solar transmittance).

the time range of liquid PCM with specific heat capacities of PCM 223, 4460, and 22,300 J/kg K are 9:50 and 315 min, 10:03 and 328 min, and 11:19 and 314 min, respectively. The above analysis indicates that increasing the specific heat capacity of PCM is not an effective method to improve the thermal performance of double-glazed units filled with PCM when the specific heat capacity of PCM is <4460 J/kg K.

3.4. Effect of latent heat

For investigating the effect of latent heat of PCM on energy performance of glazing units containing PCM, the conditions of five types of latent heat of PCM, $0.1Q_L = 20.5$, $Q_L = 205$, $2Q_L = 410$, $5Q_L = 1025$, and $10Q_L c_{p,p} = 2050$ kJ/kg, are investigated, while keeping the remaining parameters unchanged as in Table 1.

Fig. 8 shows simulation results of the interior surfaces on double-glazed units with different latent heats of PCM. As shown in Fig. 8(a), when the latent heat of PCM is 20.5, 205, 410, 1025, or 2050 kJ/kg, the temperature time lag and temperature decrement factor are 14 min and 1.00, 17 min and 1.00, 60 min and 0.97, 151 min and 0.46, and 156 min and 0.08, respectively. These results show that with the latent heat of PCM increasing, the temperature time lag increases, and the temperature decrement factor decreases; however, the effect of the latent heat of PCM on the temperature decrement factor is weak when the latent heat of PCM is <4100 kJ/kg. It is also observed from Fig. 8(a) that the temperature of the interior surface on double-glazed units changes slightly when the latent heat of PCM is >2050 kJ/kg, and the largest temperature difference in a whole day is only 0.83 °C.

From Fig. 8(b) and (c), it can be seen that the effect of latent heat of PCM on the total transmitted and solar energy of the interior surface on double-glazed units is also weak when the latent heat of PCM is beyond 1025 kJ/kg. It is found from Fig. 8(d) that with the latent heat of PCM increasing, the initial melting time is delayed, and the time range of liquid PCM is narrower; however, when the latent heat of PCM is beyond 1025 kJ/kg, the PCM is not melting, which results in lower values of solar transmittance of the double-glazed unit. For example, the initial melting time and the time range of liquid PCM with the latent heat of PCM 20.5 and 410 kJ/kg are 8:12 and 403 min and 11:18 and 234 min, respectively. The above analysis indicates that increasing the latent heat of PCM is an effective method to improve the thermal performance of double-glazed units filled with PCM when the latent heat is <410 kJ/kg.

3.5. Effect of melting temperature

The conditions of five types of melting temperature, 297–299, 300–302, 304–306, 307–309, and 309–311 K, are

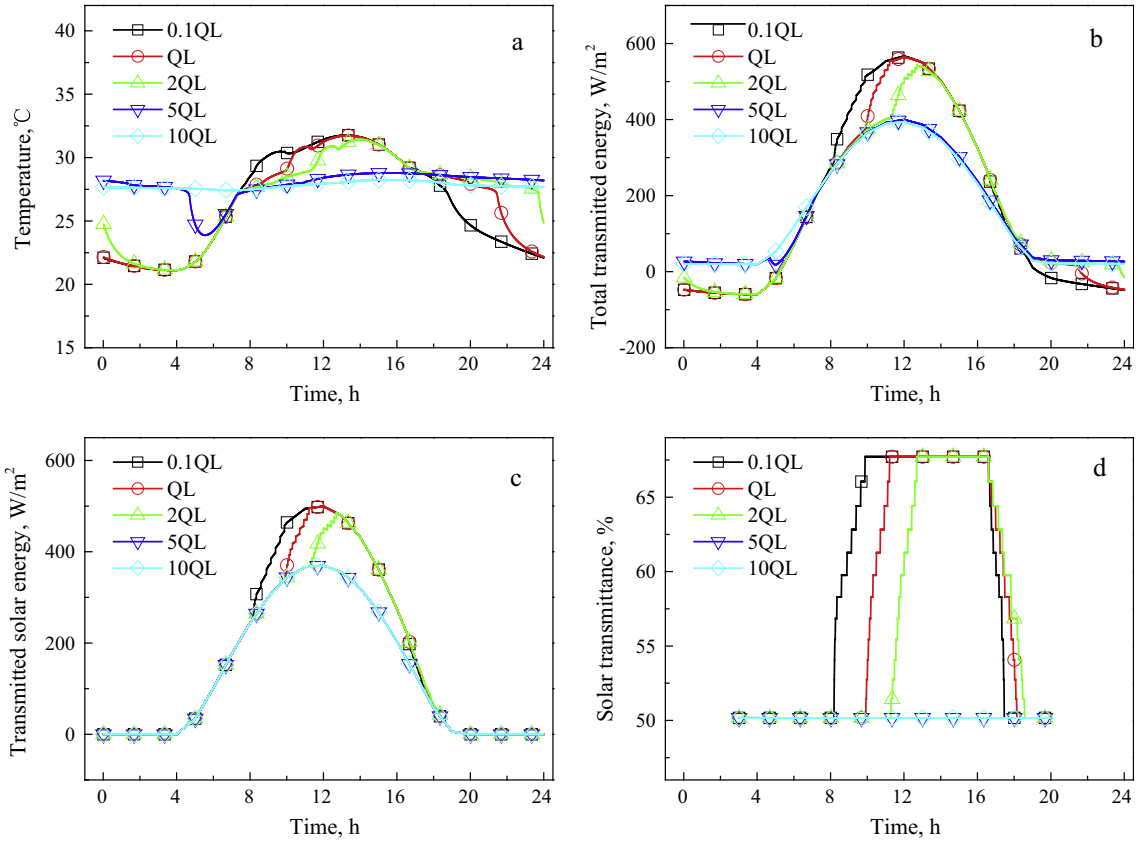

Fig. 8. Simulation results of the interior surface on double-glazed units with different latent heats of PCM (a: temperature; b: total energy; c: solar energy; d: solar transmittance).

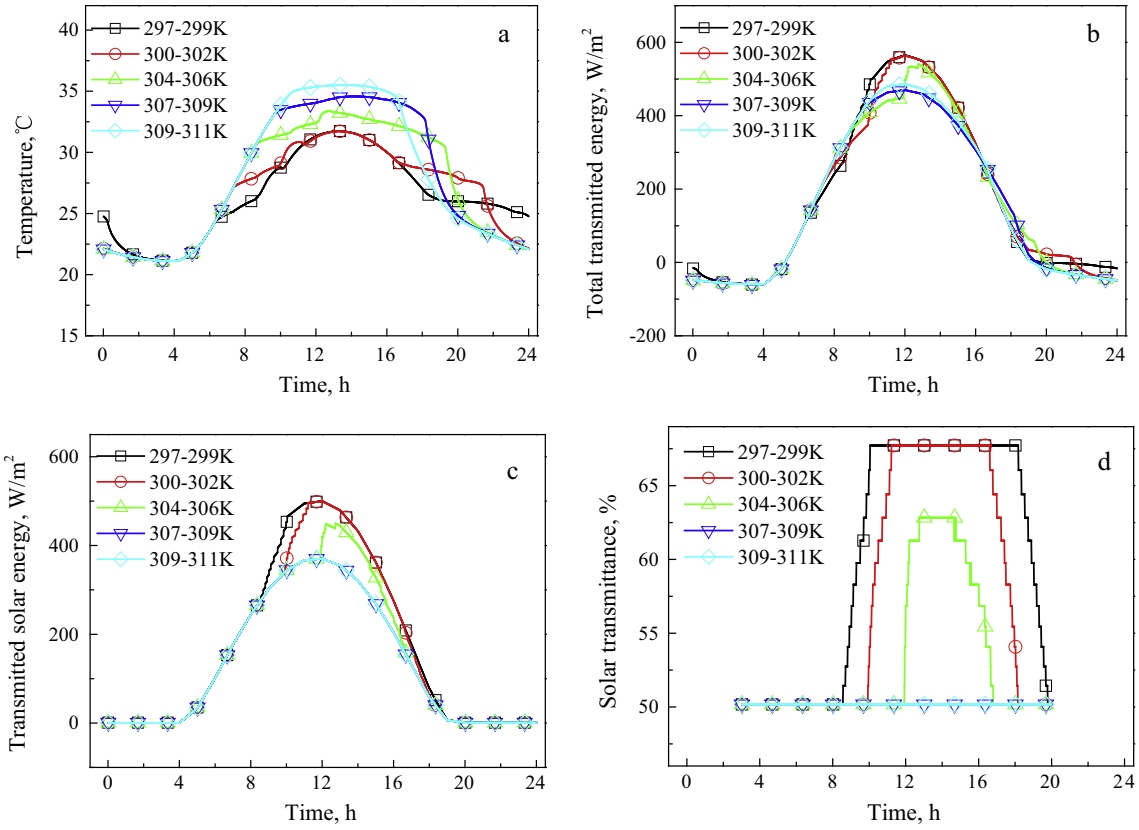

Fig. 9. Simulation results of the interior surface on double-glazed units with different melting temperature of PCM (a: temperature; b: total energy; c: solar energy; d: solar transmittance).

investigated, while keeping the remaining parameters unchanged as in Table 1.

Fig. 9 illustrates the simulation results of the interior surfaces on double-glazed units with different melting temperatures of PCM. As shown in Fig. 9(a), when the melting temperature of PCM is 297–299, 300–302, 304–306, 307–309, and 309–311 K, the temperature time lag and temperature decrement factor are 13 min and 1.00, 17 min and 1.00, 6 min and 1.16, 68 min and 1.27, and 28 min and 1.35, respectively. These results show that with the melting temperature of PCM increasing, the temperature decrement factor increases; however, the effect of the melting temperature of PCM on the temperature time lag is not regular, and the temperature decrement factor is >1.1 when the melting temperature of PCM is beyond 304–306 K. From Fig. 9(b) and (c), it can be seen that the effect of melting temperature of PCM on the total transmitted and solar energy of the interior surface on double-glazed units is also weak when the melting temperature of PCM is >307–309 K, and the total transmitted and solar energy of the interior surface on double-glazed units decrease with the melting temperature of PCM increasing when the melting temperature of PCM is <304–306 K.

It is found from Fig. 9(d) that with the melting temperature of PCM increasing, the initial melting time is delayed, and the time range of liquid PCM is narrower; however, when the melting temperature of PCM is >307–309 K, the PCM does not melt, which results in lower values of solar transmittance of the double-glazed units. For example, the initial melting time and the time range of liquid PCM with the melting temperatures of PCM 297–299 and 304–306 K are 8:34 and 487 min and 11:56 and 0 min, respectively. These results show that the PCM is only partly melting when the melting temperature of PCM is 304–306 K. The above analysis indicates that controlling the melting temperature of PCM is an effective method to improve the thermal performance of double-glazed units filled with PCM, and which should be matched not only with between indoor and outdoor temperatures, but also with solar transmittance of double-glazed units. For example, the melting temperature of PCM 297–299 K is relatively matched with the environmental conditions of Daqing.

4. Conclusions

In this study, thermal performance of a PCM-filled double-glazing unit with different thermophysical parameters of PCM in Northeast China was investigated numerically. With the aim to investigate the thermal behavior of a PCM-filled double-glazing unit, the influences of density, specific heat capacity, latent heat, thermal conductivity, melting temperature of PCM were also studied. The following conclusions can be drawn:

(1) Choosing rational density of PCM is an effective method to improve the thermal performance of double-glazed units filled with PCM; however, the solar transmittance of double-glazed units is very poor when the density of PCM is >1275 kg/m^3. With the density of PCM increasing, the temperature time lag increases, the temperature decrement factor and the time range of liquid PCM decrease, and the initial melting time is delayed; however, the effect of density of PCM on the temperature decrement factor is weak.
(2) Increasing the thermal conductivity of PCM is not an effective method to enhance the thermal performance of double-glazed units filled with PCM when the thermal conductivity of PCM is >2.1 W/m K. With the thermal conductivity of PCM increasing, when the thermal conductivity of PCM is <2.1 W/m K, the temperature time lag and the time range of liquid PCM increase and the temperature decrement factor decreases; however, when the thermal conductivity of PCM is >2.1 W/m K, the effect of thermal conductivity of PCM is clearly weak.
(3) Increasing the specific heat capacity of PCM is not an effective method to enhance the thermal performance of double-glazed units filled with PCM when the specific heat capacity of PCM is <4460 J/kg K. With the specific heat capacity of PCM increasing, the temperature time lag increases, the temperature decrement factor decreases, the initial melting time is delayed, and the time range of liquid PCM changes slightly; however, the effect of specific heat capacity of PCM is weak when the specific heat capacity of PCM is <4460 J/kg K.
(4) Increasing the latent heat of PCM is an effective method to enhance the thermal performance of double-glazed units filled with PCM when the latent heat is <410 kJ/kg. With the latent heat of PCM increasing, the temperature time lag increases and the temperature decrement factor decreases; however, the effect of latent heat of PCM on the temperature decrement factor is weak when the latent heat of PCM is <410 kJ/kg. With the latent heat of PCM increasing, the initial melting time is delayed and the time range of liquid PCM is narrower; however, when the latent heat of PCM is >1025 kJ/kg, the PCM does not melt.
(5) Controlling the melting temperature of PCM is an effective method to improve the thermal performance of double-glazed units filled with PCM, and which should be matched with not only between indoor and outdoor temperature, but also solar transmittance of double-glazed units. With the melting temperature of PCM increasing, the temperature decrement factor increases; however, the effect of the melting temperature of PCM on the temperature time lag is not regular. With the melting temperature of PCM increasing, the initial melting time is delayed, and the time range of liquid PCM is narrower. The melting temperature range of PCM 297–299 K is relatively matched with the environmental conditions of Daqing.

Acknowledgment

This study was financially supported by the National Science Foundation of China (NSFC) through Grant No. 51306031.

References

Aguilar, J.O., Xaman, J., Alvarez, G., Hernandez-Pereza, I., Lopez-Mata, C., 2015. Thermal performance of a double pane window using glazing available on the Mexican market. Renew. Energy 81, 785–794.
Arıcı, M., Karabay, H., 2010. Determination of optimum thickness of double-glazed windows for the climatic regions of Turkey. Energy Build. 42, 1773–1778.
Berthou, Y., Biwole, P.H., Achard, P., Sallée, H., Tantot-Neirac, M., Jay, F., 2015. Full scale experimentation on a new translucent passive solar wall combining silica aerogels and phase change materials. Sol. Energy 115, 733–742.
Chow, T.T., Li, C., Zhang, L., 2011. Thermal characteristics of water-flow double-pane window. Int. J. Therm. Sci. 50, 140–148.
Dai, G.L., Xia, X.L., Hou, G.F., 2014. Transmission performances of solar windows exposed to concentrated sunlight. Sol. Energy 103, 125–133.
Erdem, C., Young, C.H., Saffa, B.R., 2014. Performance investigation of heat insulation solar glass for low-carbon buildings. Energy Convers. Manage. 88, 834–841.
Erdem, C., Riffat, S.B., 2015. A state-of-the-art review on innovative glazing technologies. Renew. Sustain. Energy Rev. 41, 695–714.
Erdem, C., Young, C.H., Riffat, S.B., 2015. Thermal performance investigation of heat insulation solar glass: a comparative experimental study. Energy Build. 86, 595–600.
Goia, F., Perino, M., Haase, M., 2012a. A numerical model to evaluate the thermal behaviour of PCM glazing system configurations. Energy Build. 54, 141–153.
Goia, F., Zinzi, M., Carnielo, E., Serra, V., 2012b. Characterization of the optical properties of a PCM glazing system. Energy Procedia 30, 428–437.
Goia, F., Zinzi, M., Carnielo, E., Serra, V., 2015. Spectral and angular solar properties of a PCM-filled double glazing unit. Energy Build. 87, 302–312.
Goia, F., Bianco, L., Cascone, Y., Perino, M., Serra, V., 2014a. Experimental analysis of an advanced dynamic glazing prototype integrating PCM and thermotropic layers. Energy Procedia 48, 1272–1281.
Goia, F., Perino, M., Serra, V., 2014b. Experimental analysis of the energy performance of a full-scale PCM glazing prototype. Sol. Energy 100, 217–233.
Gowreesunker, B.L., Stankovic, S.B., Tassou, S.A., Kyriacou, P.A., 2013. Experimental and numerical investigations of the optical and thermal aspects of a PCM-glazed unit. Energy Build. 61, 239–249.
Hee, W.J., Alghoul, M.A., Bakhtyar, B., Elayeb, O., Shameri, M.A., Alrubaih, M.S., 2015. The role of window glazing on day lighting and energy saving in buildings. Renew. Sustain. Energy Rev. 42, 323–343.
Ismail, K.A.R., Henrıquez, J.R., 2002. Parametric study on composite and PCM glass systems. Energy Convers. Manage. 43, 973–993.
Ismail, K.A.R., Salinas, C.T., Henriquez, J.R., 2008. Comparison between PCM filled glass windows and absorbing gas filled windows. Energy Build. 40, 710–719.
Kimmo, H., Eerik, M., Jukka, L., 2015. Energy saving potential of glazed space: sensitivity analysis. Energy Build. 99, 87–97.

Li, D., Qi, H.B., Wu, G.Z., 2015. Determined optical constants of liquid hydrocarbon fuel by a novel transmittance method. Optik 126, 834–837.

Li, S.H., Zhong, K.C., Zhou, Y.Y., Zhang, X.S., 2014. Comparative study on the dynamic heat transfer characteristics of PCM-filled glass window and hollow glass window. Energy Build. 85, 483–492.

Liao, W., Xu, S., 2015. Energy performance comparison among see-through amorphous-silicon PV (photovoltaic) glazings and traditional glazings under different architectural conditions in China. Energy 83, 267–275.

Martin, T., Ergo, P., Jarek, K., Hendrik, V., 2013. Facade design principles for nearly zero energy buildings in a cold climate. Energy Build. 67, 309–321.

Müslüm, A., Hasan, K., Mirac, K., 2015. Flow and heat transfer in double, triple and quadruple pane windows. Energy Build. 86, 394–402.

Müslüm, A., Mirac, K., 2015. An investigation of flow and conjugate heat transfer in multiple pane windows with respect to gap width, emissivity and gas filling. Renew. Energy 75, 249–256.

Pielichowska, K., Pielichowski, K., 2014. Phase change materials for thermal energy storage. Prog. Mater. Sci. 65, 67–123.

Ron, Z., Martin, F., Luis, P.G., 2014. Thermal radiation heat transfer: including wavelength dependence into modelling. Int. J. Therm. Sci. 86, 189–197.

Takeshi, I., Steinar, G., Tao, G., Arild, G., Jelle, B.P., 2015. Impact of convection on thermal performance of aerogel granulate glazing systems. Energy Build. 88, 165–173.

Tiago, S., Romeu, V., Fernanda, R., Samagaio, A., Claudino, C., 2015a. Development of a window shutter with phase change materials: full scale outdoor experimental approach. Energy Build. 88, 110–121.

Tiago, S., Romeu, V., Fernanda, R., Samagaio, A., Claudino, C., 2015b. Performance of a window shutter with phase change material under summer Mediterranean climate conditions. Appl. Therm. Eng. 84, 246–256.

Wang, F.Q., Tan, J.Y., Ma, L.X., Shuai, Y., Tan, H.P., Leng, Y., 2014. Thermal performance analysis of porous medium solar receiver with quartz window to minimize heat flux gradient. Sol. Energy 108, 348–359.

Wang, F.Q., Shuai, Y., Tan, H.P., Lin, R.Y., 2013. Researches on a new type of solar surface cladding reactor with concentration quartz window. Sol. Energy 94, 177–181.

Wang, F.Q., Tan, J.Y., Ma, L.X., Wang, C.C., 2015. Effects of glass cover on heat flux distribution for tube receiver with parabolic trough collector system. Energy Convers. Manage. 90, 47–52.

Xamán, J., Pérez-Nucamendi, C., Arce, J., Hpnojosa, J., Álvarez, G., Zavala-Guillén, I., 2014. Thermal analysis for a double pane window with a solar control film for using in cold and warm climates. Energy Build. 76, 429–439.

Zhong, K.C., Li, S.H., Sun, G., Li, S., Zhang, X., 2015. Simulation study on dynamic heat transfer performance of PCM-filled glass window with different thermophysical parameters of phase change material. Energy Build. 106, 87–95.